BIAO SHEN
First Last

ASME Paper Title: Limited Enhancement of Subatmospheric Boiling on Treated Structured Surfaces With Biphilic Pattern

Authors: Biao Shen, Naoki Iwata, Sumitomo Hidaka, Koji Takahashi and Yasuyuki Takata

ASME Journal Title: Journal of Heat Transfer

Volume/Issue 143/10 Date of Publication (VOR* Online) Sep. 8, 2021

ASME Digital Collection URL: https://asmedigitalcollection.asme.org/heattransfer/article-abstract/143/10/101601/1 Enhancement-of-Subatmospheric-Boiling-on?redirectedFrom=fulltext

DOI: 10.1115/1.4051056

Limited Enhancement of Subatmospheric Boiling on Treated Structured Surfaces with Biphilic Pattern

Biao Shen[1]

Degree Programs in Systems and Information Engineering
The University of Tsukuba
Tennodai 1-1-1, Tsukuba 305-8573, Japan
b.shen@kz.tsukuba.ac.jp

Naoki Iwata

Department of Mechanical Engineering
Kyushu University
744 Motooka, Nishi-ku, Fukuoka 819-0395, Japan
n.iwata@heat.mech.kyushu-u.ac.jp

Sumitomo Hidaka

Department of Mechanical Engineering
Kyushu University
744 Motooka, Nishi-ku, Fukuoka 819-0395, Japan
hidaka@mech.kyushu-u.ac.jp

Koji Takahashi

Department of Aeronautics and Astronautics
Kyushu University
744 Motooka, Nishi-ku, Fukuoka 819-0395, Japan
takahashi@aero.kyushu-u.ac.jp

Yasuyuki Takata

Department of Mechanical Engineering
Kyushu University
744 Motooka, Nishi-ku, Fukuoka 819-0395, Japan
School of Engineering, The University of Edinburgh
The King's Buildings, Mayfield Road, Edinburgh EH9 3JL, United Kingdom
takata@mech.kyushu-u.ac.jp

[1] To whom correspondence should be addressed

Abstract

Boiling heat transfer suffers deteriorations under subatmospheric conditions, which can be attributed to a shortage of viable nucleation sites at declining pressures. In this work, the possibility of enhancing low-pressure saturated boiling of water using a combination of wettability patterning and structural modifications was experimentally explored. The copper test surface, comprised of an array of circular "dimples" (0.3 mm in depth, 0.5 mm in diameter, and 3.0 mm in pitch), was spray-coated by PTFE (polytetrafluoroethylene) coatings so as to form a matching biphilic pattern with the surface cavities. The resulting dimpled biphilic surface showed appreciable heat transfer enhancement—with a maximum 60% increase of the average heat transfer coefficient of nucleate boiling compared with a flat biphilic surface—down to about 9.5 kPa. Further lowering the pressure to 7.8 kPa, however, was found to lead to diminished performance gains. The visualization study of the bubble departure dynamics revealed signs of additional vapor trapping of the hydrophobic-coated cavities, which can induce uninterrupted bubble regeneration with zero waiting time and explain the qualified enhancement of subatmospheric boiling. Thanks to a potential secondary pinning of contact line inside the hydrophobic cavities, incomplete bubble detachment could prevail at somewhat lower pressures than was otherwise possible without the dimple structure, leaving behind significantly more vapor residues. However, the vapor trapping capacity was found to decrease with pressure, which provided clues with regard to the reduced efficacy of the surface at even lower pressures.

Nomenclature

a	=	slope of linear fit of the temperature distribution, $^{\circ}$C/mm
b	=	intercept of linear fit of the temperature distribution, $^{\circ}$C
C	=	constants used in empirical correlations Eqs. (1) and (2)
c_p	=	specific heat at constant pressure, kJ/kg K
D_b	=	bubble diameter at departure, mm
g	=	gravitational acceleration, m/s^2
H	=	water height, mm
h	=	heat transfer coefficient, kW/m^2 K
h_{lv}	=	latent heat of vaporization, kJ/kg
Ja	=	Jakob number
L	=	cavity diameter, mm
m	=	constant in Eq. (3)
n	=	constant in Eq. (1)
P	=	pressure, kPa
P^*	=	threshold pressure as defined by Eq. (10) and Eq. (11), kPa
Pr	=	Prandtl number
p	=	pitch, mm
q	=	heat flux, kW/m^2
Ra	=	surface roughness, μm
T_i	=	temperature measurements by heater thermocouples (i=1, 2, and 3), $^{\circ}$C

ΔT_{sat} = surface superheat, K

x_i = locations of the heater thermocouples (i=1, 2, and 3), mm

z = cavity depth, mm

Greek letters

α = thermal diffusivity, m^2/s

β = static contact angle, $^{\circ}$

δ = uncertainty

λ = thermal conductivity, W/m K

μ = dynamic viscosity, μPa s

ϱ = density, kg/m^3

σ = surface tension, mN/m

Subscripts

b = bulk fluid

c = copper heat transfer block

L = the Levy correlation

l = liquid

ONB = onset of nucleate boiling

R = the Rohsenow correlation

sat = saturated state

v = vapor

w = test surface

1. Introduction

1.1 Fundamentals of boiling heat transfer.

Heat is an integral part of modern industry, from power generation to air-conditioning and refrigeration. How to safely dissipate large amounts of industrial heat without incurring detrimental temperature excursions raises growing challenges to come up with novel efficient cooling solutions. In electronics cooling in particular, the demand is even more urgent as recent advances in miniaturization of computer components continue to elevate surface heat flux to seemingly untenable levels (projected to exceed 100 W/cm^2 [1]) that go well beyond the capabilities of conventional fan-cooled heat sinks. Two-phase cooling schemes such as boiling offer an attractive alternative to keep computer chip temperature low when continuously removing heat in a reliable and efficient manner [2]. Boiling heat transfer, by tapping into the vast reservoir of latent heat of vaporization, has the potential to provide heat transfer rates that can be orders-of-magnitude more efficient than single-phase heat conduction and convection.

Despite the apparent importance of boiling and the intense intellectual interest that it has stirred in decades past [3,4], the topic still remains a fertile research ground that seems to have more questions than clear answers. A well-established theory by Hsu [5] has heterogeneous boiling started when a bubble manages to emerge from vapor nuclei embedded in surface defects and scratches (of certain critical sizes) and moves on to grow in a sufficiently superheated liquid layer. Such onset of nucleate boiling (ONB) is marked by a sharp departure from the mode of single-phase convection on the typical boiling curve that depicts the relationship between surface heat flux q and wall superheat ΔT_{sat}. In this physical scenario, bubble nucleation relies exclusively upon the presence of trapped gas and vapor [6] and the availability of properly sized cavities [7]. The former has to do with the initial wetting state of the surface, in which, based on Bankoff's simple model [8], the advancing contact angle plays a vital role. Air trapping, however, might be subject to long-term volatility as air tends to gradually diffuse into the surrounding liquid, thus leading to the eventual flooding of the whole surface [7], which can partially explain the wide gap between actual ONB measurements and theoretical predictions [9] and the 'aging' effect that undermines the efficacy of most surface enhancement techniques [10]. The latter criterion regarding cavity size is currently facing mounting scrutiny as new experimental evidence brings to the fore questions about its physical validity. Nam et al. [11] obtained unexpectedly low ONB superheats (ΔT_{ONB} =3 K) in boiling of degassed water on a Teflon-coated hydrophobic silicon substrate that was supposedly cavity-free with a root-mean-squared (RMS) roughness less than 1 nm. Qi and Klausner [12] measured the active nucleation site density in heterogeneous boiling of highly wetting ethanol on nominally smooth and coarse surfaces, which, surprisingly, showed nearly identical results. Perplexed by the findings, they went on to propose surface nanobubbles as an alternative mechanism to the classical vapor-trapping-cavity model.

Drawing energy from the heater surface and the surrounding superheated liquid, the bubble continues to grow and finally detach itself from the surface, which is usually followed by a finite waiting period such that the nucleation condition can be met to initiate the next ebullition cycle. Major contributions to the highly efficient heat transfer during this phase of nucleate boiling include transient heat conduction as a result of repeated regeneration of a thermal layer swept away by the departing bubbles, evaporation of a liquid microlayer trapped at the base of an expanding bubble interface, and enhanced local flow motion (i.e., microconvection). Mikic and Rohsenow [13] proposed, under the assumption of heat transfer being dominated by heat conduction, an early correlation for nucleate boiling that requires extensive empirical inputs including the number of active nucleation sites, bubble departure diameter and frequency. Yet, according to a wall heat flux partitioning analysis based on numerical results, the time-integrated contribution of thermal conduction was capped at a maximum 50% and became relevant only towards the late stages of bubble departure [14].

The significance of microlayer evaporation has long been an area of debate in boiling research. The pioneering measurement of microlayer formation by Koffman and Plesset [15] using laser interferometry combined with high-speed photography revealed a typical microlayer—formed in boiling of subcooled water at atmospheric pressure on a Pyrex glass surface—to have a wedgelike profile initially about 1.85 μm thick and 0.25 mm wide. Dismissed early on as the least significant amongst the boiling heat transfer mechanisms [13], evaporation of such a finely-structured layer, as it turns out, involves complex heat and momentum transport subprocesses. In order to derive an accurate description[16–18], it requires detailed accounts for the capillary pressure, disjoining pressure and recoil pressure, which leads ultimately to a fourth-order ordinary differential equation for the layer thickness. Employing numerical simulations, Stephen and coworkers [19,20] reached the conclusion that as much as 30% of the total heat transfer could have passed through the microlayer region prior to the dry-out condition. Utaka et al. [21] performed simultaneous measurements of the evolving microlayer structure and the bubble expansion process, and reported that the contribution of microlayer evaporation was probably in the range of 14-44% for water and around 39% for ethanol, respectively.

It has long been recognized that 'agitation' to the liquid caused by oscillations of the liquid-vapor interface and, to a greater extent, vortical motion formed in the wake of a departing bubble plays a leading role in improving heat transfer efficiency. Based on a direct analogy with forced convection (with the dimensionless Reynolds number defined using the empirical values for the mass velocity and size of the bubble leaving the surface), Rohsenow [22] proposed one of the most acclaimed correlations for pool boiling in 1952,

$$\frac{c_{p,l}\Delta T_{sat}}{h_{lv}} = C_R \left[\frac{q}{\mu_l h_{lv}} \sqrt{\frac{\sigma}{g\left(\rho_l - \rho_v\right)}} \right]^{0.33} \mathrm{Pr}^n \tag{1}$$

where $c_{p,l}$ denotes the liquid specific heat, h_{lv} the latent heat of vaporization, μ_l the liquid dynamic viscosity, σ the surface tension, g the acceleration due to gravity, ϱ_l the liquid density, ϱ_v the vapor density, and Pr_l the liquid Prandtl number. The constants C_R and n depend on the specific surface-fluid combination [23]. Further modifications to the above correlation were made later by Levy [24]—who used analytical prediction for the bubble growth rate to define the Reynolds number—so as to curtail its reliance on empirical inputs. That effort arrived at

$$q = \frac{1}{C_L} \frac{\lambda_l c_{p,l} \rho_l^{\,2}}{\sigma T_{sat}\left(\rho_l - \rho_v\right)} \Delta T_{sat}^{\,3} \tag{2}$$

where C_L is a constant determined by experimental data and λ_l the liquid thermal conductivity. Note that the well-known $q \sim \Delta T_{sat}^3$ relation [6] can be recovered explicitly in Eq. (2).

A recent numerical study by Kandlikar [4] suggests that enhanced evaporation at the bubble interface is most likely a secondary effect resulting from microconvection entraining superheated liquid from the thermal layer over the rest of the bubble surface. For more on the mechanistic descriptions of boiling heat transfer, the reader is referred to the superb reviews by Dhir et al. [14] and Kim [25].

As the surface heat flux continues to rise, the isolated-bubble regime is quickly taken over, due to increasing bubble coalescence, by formation of massive structures like vapor columns and mushrooms (with stems extending to the surface), and finally by that of vapor patches (i.e., local film boiling) [26]. Through numerical simulations, Dhir et al. showed that vertical merger between successive bubbles ejected from the same nucleation site contributed little to heat transfer [27] while, by contrast, lateral merger of bubbles from neighboring sites could lead to formation of vapor bridges with liquid trapped underneath, whose evaporation was able to cause a temporary boost to the overall wall heat flux [28]. With the surface being increasingly deprived of liquid supply that fuels sustained nucleation of bubbles, boiling enters a transition to the far less efficient mode of film boiling [29,30], culminating in a dramatic event called critical heat flux (CHF). The corresponding *peak* heat flux on the proverbial boiling curve can be triggered by various mechanisms, including notably the Taylor-Helmholtz instability at the interface of escaping vapor jets [31] and the dominance of evaporation momentum force parallel to the heater surface [32,33].

1.2 Enhancement of nucleate boiling.

As pointed out by Warrier and Dhir [34], empirical curve-fitting-based correlations of boiling heat transfer are prone to gross errors, whose predicting power tends to fall precipitously when applied to situations outside their designed limits, due largely to a lack of sound physical foundation. Yet the mechanistic approach [6], as a result of its normally narrow scope, also faces challenges of inconsistency as it often fails to take into account the complex interactions between various relevant subprocesses involved in nucleate boiling. For these reasons, there genuinely is an epistemic divide between the physical interpretation of boiling and how that knowledge can be used to improve it in practice. Answers to the latter question, decades of continuous efforts notwithstanding, are still being sought mostly through trial-and-error measures, which makes boiling heat transfer enhancement more of an art than an exact science.

Increasing surface roughness is one of the most basic techniques to enhance nucleate boiling. One can create more vapor-trapping cavities simply by roughening the surface, which would likely have an augmented bubble population (and larger heat transfer area) and consequently a higher heat transfer coefficient. However, the practice has its limitations. First, diminished returns with further increasing roughness have been well documented in experiments. Jones et al. [35] reported little improvement to the heat transfer coefficient of pool boiling of water on test surfaces modified by electrical charge machining beyond a threshold around 1.08 μm; Kim et al. [36] found CHF to rise before plateauing with increasing roughness of superhydrophilic aluminum surfaces, in spite of the apparently augmented capillary wicking due to the formation of nanoscale-protrusion structures. Second, cavities formed by scuffing and roughening the surface are known to be vulnerable to *flooding* (by highly-wetting fluids in particular) [6,7], which contributes to the long-term performance degradation known as 'the aging effect' [10].

In order to build more stable vapor traps, multiple studies have been devoted to designs of reentrant-type surfaces with complicated three-dimensional structures. The famous 'pore-and-tunnel' surface geometry [37], for instance, helps significantly enhance (latent) heat transfer by continuously drawing liquid through the open pores in the surface into the interconnected tunnel space underneath, where it comes into contact with heated surface over a larger area and quickly evaporates [10]. Li and Peterson [38] developed microporous boiling surfaces by sintering multilayer isotropic copper wire screens. The fused meshes formed the highly conductive skeleton of the porous media, via which heat could be transported more efficiently to the numerous nucleation sites on the surface. Interestingly, they noted that the seemingly dry-out condition inside the porous structure did not automatically trigger CHF, thanks to an alternative route somehow opened up for vapor escape through the unsealed sides of the coating. More direct manipulation of vapor and liquid pathways were attempted by use of microchannel surfaces [39] and bi-conductive surfaces [40]. Surface wettability patterning in particular has emerged as one of the most promising ways to actively manipulate bubble behavior. In general terms, hydrophobic surfaces (with a contact angle β>90°) promote bubble formation while liquid wetting is facilitated if the surface is hydrophilic (β<90°). A hybrid surface endowed with these two opposing topographical characteristics is capable of bringing about a higher degree of control over bubble growth and spreading in nucleate boiling, which can be optimized to achieve more effective boiling heat transfer [41]. Betz et al. [42] first discovered that the maximum heat flux and heat transfer coefficient of saturated boiling of water could be enhanced, respectively, by a significant margin of 65% and 100% when a non-connected network of Teflon hydrophobic hexagonal patterns were deposited on a hydrophilic silicon wafer. (Such surface feature has since been coined *biphilicity*). Aside from spatially juxtapositions of wettability patterns, Frankiewicz and Attinger [43] raised an interesting concept of *temporal* biphilicity where reversible switches between the hydrophilic Wenzel state and the hydrophobic Cassie-Baxter state could be made by special repeated protocols of overheating and pressurization of the surface.

One often overlooked feature of biphilic surfaces has to do with the ease with which bubbles get nucleated [44]. It has long been established that wettability is a singularly important surface parameter affecting bubble nucleation. Wang and Dhir [45] found that a decrease from β=90^{o} to 18^{o} (caused by oxidation of the test copper surface) resulted in over a 90% drop in the active site density and noticeably lower heat transfer rates. The exceptionally low ONB, along with essentially no waiting time, of hydrophobic surfaces [11] proved to be of great asset to boiling at subatmospheric pressures, which could be particularly susceptible to debilitating performance deterioration known as intermittent boiling (even on enhanced microchannel surfaces [2]). We previously studied low-pressure boiling on flat biphilic surfaces that were electroplated with hydrophobic nickel and TFEO (tetrafluoroethylene oligomer) spots [46]. The results showed that the transition to the regime of intermittent boiling was effectively delayed—owing to the robustness of nucleation sites to pressure reductions as a result of strong pinning of the bubble contact line [47]—but not completely eliminated. The objective of the present study is to explore the possibility of inducing greater enhancement of nucleate boiling at very low pressures on biphilic surfaces by means of incorporating cavity structures. The results show that surface 'dimples' overlapping with hydrophobic patterns can provide much stable traps for vapor residues and act as more reliable nucleation sites than flat biphilic surfaces.

2. Experimental setup

2.1 Boiling facility.

A schematic diagram of the boiling test rig is shown in Fig. 1. The Pyrex-glass boiling vessel had an inner diameter of 120 mm and a height of 450 mm. The top plate of the vessel consisted of ports for a pressure gauge and a K-type thermocouple (1.0 mm in diameter) that were employed to measure the pressure and pool temperature, respectively. A thermodynamically saturated state of the bulk working fluid—deionized pure water in this case—was maintained during experiments by manually adjusting two coil heaters (powered by variable voltage transformers) and an internal cooler (connected to a constant-temperature water chiller, with a maximum cooling power of 360W). The vessel itself was placed in a case made of Styrofoam (with a glass window installed for visualization purposes). A PID-regulated air heater (with a maximum output of 0.14 m^3/min@600 °C) was relied on to mitigate any potential heat losses to the environment.

The vessel bottom was attached to the heater assembly that contained an ⌀30-mm copper heat transfer block (about 100 mm long). Wrapped in glass wool insulation, the heat transfer block had a tapered lower body (for mounting ease). The upper-facing surface of the block was used as the test surface, which was widened to include a thin (0.3 mm) 50-mm-wide ring so as to effectively suppress unwanted bubble nucleation at the edges. The installation of the block was secured by an O-ring, and adhesive silicon RTV sealant was applied at the groove between the ringed surface and the stainless casing—and allowed to cure overnight—before each experimental run. Two sheath heaters (with a maximum power of 700 W each) were embedded in the copper base of the heater assembly to provide a continuous heat load to the heater surface. Minimal (radial) heat losses were deemed for one-dimensional heat conduction to prevail along the heat transfer block. Three ⌀1.0-mm K-type thermocouples (with a measurement error of ±0.12 K according to the data sheet provided by the manufacturer) were placed along the centerline of the heat transfer block, respectively, at x_1=3.9 mm, x_2=8.3 mm, and x_3=12.8 mm from the top test surface, whose readings were relied on to generate an accurate axial temperature profile. The corresponding thermocouple signals T_1, T_2, and T_3, along with the bulk temperature measurement T_b, were recorded by a Data

Acquisition system at a sampling rate of 5 s^{-1}. More technical details about the experimental setup can be found in our previous work [47].

2.2 Test surfaces.

Surfaces with overlapping wettability and cavity patterns were fabricated taking the following steps (see Fig. 2(a)). First, the top of the heat transfer block was polished to a mirror finish ($Ra \approx 0.03$ μm, using grit 600 emery paper and then buffing with 3.0 μm and 1.0 μm abrasive alumina compounds). Next, an array of 'dimples' were drilled onto the surface using a computer-aided precision desktop mill. The machined circular cavities, formed in a uniform unstaggered array of pitch p=3.0±0.01 mm (see Fig. 2(b)), all had the same diameter L=0.5±0.01 mm and depth z=0.3±0.01 mm. The bottom of the cavities was mostly flat with a roughness about $Ra \approx 4.4$ μm, as shown in Fig. 2(c).

After being washed in an ultrasonic bath of acetone, the surface cavities were spray-coated with hydrophobic PTFE (polytetrafluoroethylene) coating, with the aid of masking tape (Fig. 2(a)). The coating robustness was increased by the thermal treatment of baking the surface in an oven filled with nitrogen gas (so as to prevent oxidation) at 260 °C for over 30 minutes. The coated cavities featured a slightly elevated roughness of $Ra \approx 5.1$ μm (see Fig. 2(c)), which, along with the increased contact angle $\beta > 120^{o}$ (vs. $\beta \approx 80^{o}$ for the uncoated copper surface), makes for preferred sites for bubble nucleation. It should be noted that due to the low thermal conductivity of PTFE (around 0.25 W/m K), a significant temperature drop could potentially take place, reaching 2.5 K for a 6.4-μm [47] coating layer under a moderate surface heat flux of q=100 kW/m^2. To investigate the effect of the cavity array, we have also prepared a *flat* biphilic with an identical wetting pattern (namely, comprised of hydrophobic spots 0.5 mm in diameter and 3.0 mm in pitch).

2.3 Experimental procedure.

Deionized pure water was filled through the lower inlet opening (Fig. 1) into the boiling vessel that was evacuated by a vacuum pump, until the water reached a set height of H=120.0±1.0 mm above the heater surface. Prior to the experimental, purging the water of incondensable gas was performed by continuous vacuum deaeration for over 2 hours. From this point forward, the vessel was closed off from the atmosphere. The bulk temperature (and pressure) was allowed to gradually increase by turning on the auxiliary bulk heaters. As the readings from the pressure gauge and the pool thermocouple approached their respective target values, the power outputs of the heaters were carefully adjusted to stabilize the bulk pressure and temperature. During the experiment, the internal cooler was also used to maintain a constant background of thermal equilibrium. The experiment commenced when the fluctuations of T_b remained less than 0.5 ^{o}C over a period of 200 seconds.

We set out to study heat transfer of saturated nucleate boiling at different pressure levels. As Table 1 shows, the thermophysical properties of water experience significant variations with decreasing pressure [48], especially in the cases of μ_l and Pr_l. According to Eq. (1), boiling heat transfer can thus be expected to appreciably deteriorate under subatmospheric pressures. Also contributing (indirectly) to the poor performance is the markedly lower vapor density ϱ_v, which has been found to lead to unstable *intermittent* bubble nucleation events [46,47].

Experiments were conducted with stepwise increasing heat flux at the boiling surface under the same saturated pressure. At least 20 minutes were allowed to elapse between measurements in order to guarantee that the boiling process would reach a steady state. It is noted that all the experimental runs were terminated before CHF was triggered to avoid damages to the test surface. Also, the potential effect of boiling hysteresis was not examined in the present study since no significant temperature overshoot associated with the onset of boiling was observed (all thanks to the apparently facilitated bubble nucleation on the hydrophobic-coated surfaces [44]).

2.4 Data reductions.

The temperature readings of the embedded thermocouples T_1, T_2, and T_3—averaged over a period of 2 minutes (with limited fluctuations$<$0.25 K)—are relied on to provide a measure of steady-state heat transfer of nucleate boiling. Under the assumption of predominant Fourier heat conduction, simple least squares regression analysis leads to a temperature profile along the heat transfer block, $T(x)=ax+b$, where a and b are the fit parameters. Hence, the surface heat flux can be calculated as

$$q = \lambda_c a = \lambda_c \frac{3\sum x_i T_i - \sum x_i \sum T_i}{3\sum x_i^2 - \left(\sum x_i\right)^2} \tag{3}$$

where the copper thermal conductivity exhibits a temperature dependence as λ_c=399.1688-4.2986×10^{-2}×$\bar{T}$-2.0756×10^{-5}×$\bar{T}^2$ (in W/m K), with the overbar representing the average temperature of T_1, T_2 and T_3. The surface temperature, on the other hand, is directly extrapolated from the linear relation,

$$T_w = b = \frac{1}{3}\left(\sum T_i - a\sum x_i\right) \tag{4}$$

As for the superheat, the following definition is used

$$\Delta T_{sat} = T_w - T_{sat}\left(P_w\right) = T_w - T_{sat}\left(P_b + \rho_l g H\right) \tag{5}$$

Note that given that hydrostatic pressure could become potentially significant under low pressures, the saturation temperature is evaluated at the heater surface. Here P_b represents the system pressure measured by the pressure gauge (with a measurement error around 400 Pa). In the following, without otherwise specified, P is referred to as the pressure corrected for the hydrostatic pressure contribution. The heat transfer coefficient is simply given as

$$h = \frac{q}{\Delta T_{sat}} \tag{6}$$

The uncertainty analysis is conducted following the principle of error propagation, which ultimately arrives at

$$\delta(q)=\sqrt{\left(\frac{\partial q}{\partial \lambda_c}\delta(\lambda_c)\right)^2+\left(\frac{\partial q}{\partial a}\delta(a)\right)^2} \tag{7}$$

$$\delta(\Delta T_{sat})=\sqrt{\left(\frac{\partial \Delta T_{sat}}{\partial b}\delta(b)\right)^2+\left(\frac{\partial \Delta T_{sat}}{\partial P_b}\delta(P_b)\right)^2} \tag{8}$$

for the heat flux and superheat, respectively. Figure S1 in Supplemental Material plots a data collection of the relative uncertainties $\delta(q)/q$, $\delta(\Delta T_{sat})/\Delta T_{sat}$, and $\delta(h)/h$. All the results are estimated at 68 percent confidence level. It is made clear that with the exception of a couple of data points in the low-heat-flux region, most of the measurements are reasonably accurate, within 20% in the case of q and 10% of ΔT_{sat}, respectively. Similarly, the uncertainty for the heat transfer coefficient is evaluated using

$$\delta(h)=\sqrt{\left(\frac{\partial h}{\partial q}\delta(q)\right)^2+\left(\frac{\partial h}{\partial \Delta T_{sat}}\delta(\Delta T_{sat})\right)^2} \tag{9}$$

which is below 15% in the region of nucleate boiling.

3. Results

3.1 Plain surface.

In Fig. 3 we plot the boiling curves obtained for a plain smooth copper surface at two differing pressure levels of P=101.3 kPa (blue square) and 9.1 kPa (black circle). Also included in the figure are predictions based on Rohsenow's correlation (Eq. (1)), with the parameters C_R=0.015 and n=1.0 (chosen for the fluid-surface combination of water and circular copper plate [23]). The present experiment results show generally good agreement with the correlation. Once boiling is initiated on the plain surface, the curve for P=9.1 kPa quickly trends upwards before settling within a deviation of 10% of the empirical correlation, whereas the difference grows somewhat, to about 20% for P=101.3 kPa. Both the experiment results and the correlation demonstrate a significant deterioration of heat transfer due to the pressure decrease. The unmistakable rightward shift of the boiling curve is accompanied by an even greater jump (over 10 K) in ONB superheat, which could be largely attributed to a dearth of properly sized cavities on the surface that are able to accommodate the increasingly larger bubbles under reduced pressures [5].

3.2 Flat biphilic surface.

Figure 4 shows the boiling curves for the *flat* biphilic surface under the particularly low pressures of P=14.3 kPa (black circle), 9.5 kPa (blue triangle), and 7.8 kPa (red square). (For the sake of brevity, only experimental data subsequent to ONB are included.) Independent of pressure level, nucleate boiling is found to be generally more efficient in transporting heat on the wettability-patterned surface, which follows the same pattern of behavior as in our previous study [46]. A clear trend emerges, however, that the boiling enhancement turns less significant at lower pressures, as indicated by the visible shift of the boiling curves to the right. As was elucidated in [47], the lessening effectiveness of the biphilic surface when pressures decreases sufficiently low might have to do with deactivation of nucleation sites due to flooding of the hydrophobic spots, which has been known to occur more frequently under reduced pressures.

Moreover, it is worth noting that the enhancement appears to also be more pronounced in the low to middling heat-flux range. As shown in Fig. 5, the ratio of the heat transfer coefficient h to that based on the Rohsenow correlation (Eq. 1), h_R, reaches as high as 1.74 in the case of P=14.3 kPa when boiling is initiated. With increasing q, however, the gains in the heat transfer efficiency become less impressive, even falling below the baseline h_R for P=14.3 and 9.5 kPa towards the end of the range of heat flux in question. Such uneven enhancement of boiling heat transfer could be partially ascribed to the very manner that boiling enhancement comes to be in the first place. Boiling on the biphilic surface, because of the hydrophobicity-induced favorable condition for ebullition, is likely to feature a large bubble population (and high heat transfer rates as a result) even at very low heat fluxes, which depends closely on the specific biphilic pattern itself. The tendency for bubble nucleation to be limited to the hydrophobic part of the surface, however, could instead prove to be a hinderance under higher heat fluxes where a greater bubble population is often needed to maintain the high heat transfer coefficient. The seemingly less significant drop in h/h_R at the lower pressures (see Fig. 5) probably results from the already prevalent lack of available nucleation sites on the surface at all heat flux levels due to the transition to intermittent boiling.

3.3 Dimpled biphilic surface.

The incorporation of machined cavity structures on top of the wetting pattern can engender even greater enhancement of nucleate boiling, as is shown in Fig. 6 which depicts the boiling curves for the dimpled biphilic surface for the commensurate pressure conditions P=14.4 kPa (black circle), 9.5 kPa (blue triangle), and 7.8 kPa (red square). The gap between the experimental and the empirical results are found to have grown considerably wider, especially in the case of P=14.4 kPa (cf. Fig. 4). The average ratio of the heat transfer coefficients rises, respectively, to h/h_R=1.95 from 1.22 for P=14.4 kPa and to h/h_R=1.59 from 1.26 for P=9.5 kPa, based on the data shown in Fig. 7. It is interesting to note that the added benefit of the cavities seems to decline steeply with decreasing pressure as the average h/h_R=1.24 hardly budges in the case of P=7.8 kPa (versus h/h_R=1.26 in the flat case, see Fig. 5). In the following section, we will delve deeper to elucidate the physical mechanism that is responsible for the heat transfer enhancement.

4. Discussion

4.1 Bubble departure dynamics.

Given the relative shallowness (z=0.3 mm) and the limited quantity (76 in total) of the dimple cavities, the increase of the potential heat transfer area is estimated to be a mere 1.8% compared with the total area of the flat surface and therefore cannot account for the higher heat transfer coefficients observed. In order to better understand the differences between the boiling characteristics on the flat and dimpled biphilic surfaces, we conducted additional measurements of bubble dynamics using high-speed imaging (Vision Research Phantom v4.3 camera equipped with an AF Nikkor 180 mm f/2.8D IF-ED telephoto lens). Figure 8(a) shows the test surface used for such visualization effort, which consisted of two PTFE-coated circular cavities of dissimilar depths, z_1=1.0±0.01 mm versus z_2=0.5±0.01 mm (see Fig. 8(b)). They were placed at a distance of 15 mm apart across the center of the surface such that bubble nucleation and growth at either site could proceed with minimal interaction with the other. A cavity diameter L=1.8±0.01 mm was chosen for both cavities, which was notably larger than in the heat transfer experiments so as to provide a clearer view with finer details of bubble behavior, especially close to the heater surface. For comparison, we also measured the bubble behavior on a flat surface coated with a single hydrophobic spot with the same size.

The visualization experiments were conducted following the same protocol as in the previous measurements of boiling heat transfer. Figures 9 and 10 show the high-speed photos—captured at a frame speed of 1000 s^{-1}—that depict the critical moments before and after bubble departure from the flat and dimpled biphilic surfaces, respectively. It is noted that the heat input to the test surface was varied slightly between measurements, resulting in an average superheat around ΔT_{sat}= 7.9 K in Fig. 9 and ΔT_{sat}=8.4 K in Fig. 10, respectively.

It has been known for some time [11,44] that bubble growth on a hydrophobic surface is often preceded by nearly unrestrained expansion of the bubble base (to the point where boiling could easily be overtaken by a quasi-film boiling regime [49]). As shown in Fig. 9(a), at atmospheric pressure (P=100.8 kPa), the footprint of the bubble seems to envelop the entire hydrophobic-coated surface leading up to its final liftoff, with the bubble contact line essentially overlapping with the border with the surrounding hydrophilic copper surface. The sequence of bubble departure begins with rapid contraction of its mid-section as the base still remains attached to the surface, which leads to *necking*—one of the distinct features of bubble dynamics in boiling on hydrophobic surfaces. The thinning eventually gives rise to a rupture. Most of the bubble manages to escape due to buoyancy effect while a significant portion is left behind (marked by yellow rectangle). The residual vapor clinging to the hydrophobic spot, from which new bubbles are able to emerge with essentially no delay in time, is arguably one of the key factors in how boiling receives extra boost on biphilic surfaces [41].

At (substantially) subatmospheric pressures (P=25.3 kPa), as shown in Fig. 9 (b), one critical difference stands out—no residual vapor appears to exist in the aftermath of the bubble departure. The hydrophobic spot (circled in red) becomes fully ‘exposed’—bare of any vapor coverage—immediately after the bubble takes off from the surface. The base of the bubble, whose receding triple-phase contact line seems to have finally given in to the appreciably accelerated bubble expansion [50] to be completely dislodged from its pinned location at the edge of the hydrophobic area, finds itself being swept away along with the rest of the departing bubble. As a direct impact of the elimination of vapor residues, bubble re-nucleation from the flooded hydrophobic spot now entails slow reformation of the superheated liquid layer, in much the same way as what would occur on an uncoated plain surface. The resulting nonzero waiting time is believed to be responsible for the particularly subdued boiling under the low-pressure conditions (see Fig. 5) that barely performed above the empirical prediction.

In the case of the dimpled biphilic surface, on the other hand, a more consistent pattern of bubble departure dynamics emerges between the two pressures of P=101.4 kPa and 25.4 kPa. As is evidenced by Fig. 10(b), under a similar reduction of pressure as in the previous flat case, the hydrophobic-coated cavities still manage to retain residual vapor post departure (albeit in appreciably smaller amounts compared with Fig. 10(a)). One of the consequences of combining cavity structure with surface hydrophobization, as the results indicate, is to create substantially stronger traps for vapor that can sustain in the event of bubble departure at low pressures. We further argue that the dimpled hydrophobic spots—kept 'dry' constantly—provide significantly more stable sites for *continuous* cyclic bubble regeneration than flat hydrophobic spots, which is deemed to be a major driver responsible for the enhanced heat transfer rates shown in Fig. 7. (Incidentally, it would seem that the cavity depth plays no vital role in affecting bubble dynamics because little difference can actually be discerned between the results for z_1=1.0 mm and z_2=0.5 mm. That appears to be the case, at least, for the limited data available here. It goes without saying that more experiments are needed to derive a more definitive account of the effect.) In the next section, we seek more quantitative evidence of such enhanced trapping of vapor.

4.2. Secondary pinning of contact line.

Figure 11 represents a plot depicting the distribution over different pressures of the departure diameter D_b—which was measured by averaging the long and short axes of the departing bubble—of bubbles growing on the flat hydrophobic spot (L=1.8 mm) under the consistent superheating ΔT_{sat}= 7.9 K. Each data point (black circle) represents the median value derived from the measurements of at least eight individual bubbles, with error bars denoting the spread of the data set (namely, the maximum and minimum values of the data set). It can be seen from the figure that with decreasing pressure, D_b exhibits an interesting transition from staying mostly constant to embarking on a path leading to a sudden divergence (which is also accompanied by a proliferation of size fluctuations).

The changing behavior can be best described as a fundamental shift in bubble departure mechanics, in which contact-line dynamics plays the crucial role. Under the assumption of the contact line remaining pinned on the surface throughout the process of bubble departure, the force balance between the driving buoyancy force and the opposing surface tension force would give rise to a critical bubble size at departure in the form of

$$D_b = \left[\frac{6\sigma L}{g\left(\rho_l - \rho_v\right)} \right]^{1/3} \tag{10}$$

(Note that the size of the bubble base is taken to be the same as that of the hydrophobic spot.) The results by Eq. (10), represented by the solid line in Fig. 11, are shown to be nearly independent of pressure variations.

On the other hand, in the scenario that the contact line (namely, the bubble base) is allowed to freely contract as it faces little resistance from any potential surface heterogeneities, bubble departure would most likely depend on how much hydrodynamic drag the ascending bubble needs to overcome. That leads to a quite different formula for the departure diameter,

$$D_b = \left[\frac{9\rho_l \alpha_l}{8\pi g\left(\rho_l - \rho_v\right)} \right]^{0.5} \frac{\rho_l c_{pl} \Delta T_{sat}}{h_{lv} \rho_v} \tag{11}$$

where α_l is the liquid thermal diffusivity. In sharp contrast to Eq. (10), the above equation predicts D_b to be strongly dependent on pressure (see the dot-dash line in Fig. 11). Details about the derivations of these two models can be found in [47].

Equations (10) and (11) portray two opposite cases of bubble departure under the influence of contact-line dynamics, which seems to capture reasonably well the evolution of the measured D_b over pressure. This encouraging agreement lends support to our interpretation of how the bubble departure process on the flat biphilic surface varies with pressure. To summarize, as shown in Fig. 12(a), at relative high pressures, the expansion of the bubble footprint is mostly limited to the extent of the hydrophobic spot. Even as the bubble begins to depart the surface, the contact line is still firmly anchored to the border dividing the hydrophilic and hydrophobic regions, which leads to incomplete bubble detachment and bubble residues remaining on the hydrophobic surface. At low pressures (Fig. 12(b)), on the other hand, the weakened pinning of the contact line allows the bubble base to continuously shrink. Consequently, the bubble of considerably enlarged size leaves from the surface as a whole, leaving the hydrophobic spot fully flooded.

For bubbles emerging from the hydrophobic-coated cavities, the particular pressure dependence of D_b suggests a somewhat different route for bubble departure. In Fig. 13(a) and 13(b) we show the results for the cavities of z_1=1.0 mm and z_2=0.5 mm, respectively. It can be seen that in both cases, the average size of departing bubbles goes through two distinct stages—in large part following the pinned-contact-line model (Eq. (10)) for higher P, and the depinned-contact-line model (Eq. (11)) for lower P—in a similar way as with the flat biphilic surface. What is remarkable about these results is the apparently delayed transition from the former to the latter. Regardless of the cavity depth, D_b manages to stay relatively unchanged at pressure levels as low as about 30 kPa. In comparison, for the flat surface with similar biphilic pattern and superheating, the divergence of D_b seems to occur around a threshold pressure P^{*}=45.0 kPa (see Fig. 11) which is defined as the intersection point between the curves by Eq. (10) and Eq. (11).

This extended range of applicability—marked in red in Fig. 13(a) and 13(b)—of the pinned-contact-line model in describing the event of bubble departure, we argue, is due to what can be termed "secondary contact-line pinning" inside the hydrophobic cavity. Since the PTFE coating was applied to both the bottom and side walls of the cavity, it is reasonable to suspect that underneath a growing bubble, the entire cavity would be filled with vapor, with the contact line possibly extended as far as the cavity edge. As shown in Fig. 14(a), when the moment of departure approaches, with the contact line firmly pinned (at relatively high pressures), we expect the bubble detachment to progress similarly to that on the flat surface (Fig. 12(a)), which includes namely, necking to be followed by partial departure of the bubble. When pressure declines below P^*, the contact line could instead become increasingly prone to receding from its original position atop the cavity during bubble departure. The hydrophobic nature of the coated inside of the cavity (β>120°), however, is likely to create conditions that enable trapping of vapor in the corners after the passing of the wetting front, leading to formation of a new contact line at the bottom of the cavity (see Fig. 14(b)). The latter outcome constitutes a *secondary* contact-line pinning that can, as a result, cause premature bubble detachment from the surface (in contrast to the clean departure seen in Fig. 12(b)). Therefore, the pinned-contact-line description by Eq. (10) can to a certain degree still apply below P^* in Fig. 13(a) and 13(b).

The trapped vapor inside the cavity, we should again emphasize, is indispensable to uninterrupted cycles of bubble regeneration and growth. In Fig. 15 we map the occurrence of residual vapor over a grid defined by the cavity depth z and the reduced pressure P/P^* (with a maximum measurement uncertainty$<$2%), based on a thorough analysis of the high-speed images. As the results show, for the flat biphilic surface (z=0), the observed instances (black circle) where the hydrophobic spot was covered in vapor at the end of the last cycle of ebullition are all limited to $P>P^*$. On the other hand, residual vapor has been found to exist on the cavity-structured surfaces even at pressures noticeably below P^*. That leads us to conclude that, it is through creating more stable nucleation sites—which can reliably remain active by resisting flooding—that boiling heat transfer was substantially enhanced on the dimpled biphilic surface at low-pressure conditions (as evidenced in Fig. 7). It should also be noted, nevertheless, that at exceptionally lower pressures, even the hydrophobic-coated cavities would become vulnerable to inevitable flooding (marked by gray triangle), which might explain, for instance, the markedly reduced potency of the surface when pressure was lowered to P=7.8 kPa in Fig. 6.

5. Conclusions

In this paper, we have investigated saturated boiling on the surfaces with spatially superimposed wettability patterns and dimple structures under strongly subatmospheric conditions. Compared with the flat copper surface with the same biphilic pattern, the surface with an array of circular PTFE-coated cavities showed remarkably higher heat transfer rates, at least down to the pressure P=9.5 kPa. However, the boiling enhancement was found to be nearly exhausted when the pressure was further reduced. The limited heat transfer enhancement was attributed to the apparently improved capacity of vapor traps that were created by the hydrophobic cavities. The high-speed visualization of the bubble departure dynamics revealed that compared with the flat surface, significantly more vapor residues were retained by the dimpled biphilic surface immediately after bubble departure, which facilitates continuous ebullition cycles with zero waiting time and is vital to achieve higher heat transfer coefficient. Moreover, for the dimpled biphilic surface, the varying bubble departure diameter with decreasing pressure exhibited a somewhat delayed transition to a regime dominated by contact line depinning. Such interesting findings suggest that the bubble detachment could entail a complicated process of secondary pinning of contact line inside the hydrophobic cavity.

The mapping of the vapor trapping behavior showed the pressure limit was effectively reduced thanks to the dimpled biphilic surface. A worthwhile future extension of the current effort might include exploration of the possibility of building even stronger traps for vapor using more elaborate cavity geometry and/or superhydrophobic coatings. Furthermore, a more informed understanding of the complex contact line dynamics—which can only be provided by direct experimental access to the contact-line region—would certainly beget new insights with regard to how to completely eliminate boiling deteriorations under declining pressures.

Acknowledgement

This work was supported by JSPS KAKENHI Grant numbers 20H02088 and 20K04312.

References

[1] Mudawar, I., 2013, “Recent Advances in High-Flux, Two-Phase Thermal Management,” J. Therm. Sci. Eng. Appl., **5**(2), p. 021012.

[2] Kalani, A., and Kandlikar, S. G., 2013, “Enhanced Pool Boiling With Ethanol at Subatmospheric Pressures for Electronics Cooling,” J. Heat Transfer, **135**(11), p. 111002.

[3] Dhir, V. K., 2019, “Advances in Understanding of Pool Boiling Heat Transfer—From Earth on to Deep Space,” J. Heat Transfer, **141**(5), p. 050802.

[4] Kandlikar, S. G., 2019, “A New Perspective on Heat Transfer Mechanisms and Sonic Limit in Pool Boiling,” J. Heat Transfer, **141**(5), p. 051501.

[5] Hsu, Y. Y., 1962, “On the Size Range of Active Nucleation Cavities on a Heating Surface,” J. Heat Transfer, **84**(3), pp. 207–213.

[6] Dhir, V. K., 2006, “Mechanistic Prediction of Nucleate Boiling Heat Transfer–Achievable or a Hopeless Task?,” J. Heat Transfer, **128**(1), pp. 1–12.

[7] Qi, Y., and Klausner, J. F., 2005, “Heterogeneous Nucleation with Artificial Cavities,” J. Heat Transfer, **127**(11), pp. 1189–1196.

[8] Bankoff, S. G., 1958, “Entrapment of Gas in the Spreading of a Liquid over a Rough Surface,” AIChE J., **4**(1), pp. 24–26.

[9] Jo, H., Kaviany, M., Kim, S. H., and Kim, M. H., 2014, “Heterogeneous Bubble Nucleation on Ideally-Smooth Horizontal Heated Surface,” Int. J. Heat Mass Transf., **71**, pp. 149–157.

[10] Webb, R. L., 2004, “Donald Q. Kern Lecture Award Paper: Odyssey of the Enhanced Boiling Surface,” J. Heat Transfer, **126**(6), pp. 1051–1059.

[11] Nam, Y., Wu, J., Warrier, G., and Ju, Y. S., 2009, “Experimental and Numerical Study of Single Bubble Dynamics on a Hydrophobic Surface,” J. Heat Transfer, **131**(12), p. 121004.

[12] Qi, Y., and Klausner, J. F., 2006, “Comparison of Nucleation Site Density for Pool Boiling and Gas Nucleation,” J. Heat Transfer, **128**(1), pp. 13–20.

[13] Mikic, B. B., and Rohsenow, W. M., 1969, “A New Correlation of Pool-Boiling Data Including the Effect of Heating Surface Characteristics,” J. Heat Transfer, **91**(2), pp. 245–250.

[14] Dhir, V. K., Warrier, G. R., and Aktinol, E., 2013, “Numerical Simulation of Pool Boiling: A Review,” J. Heat Transfer, **135**(6), p. 061502.

[15] Koffman, L. D., and Plesset, M. S., 1983, “Experimental Observations of the Microlayer in Vapor Bubble Growth on a Heated Solid,” J. Heat Transfer, **105**(3), pp. 625–632.

[16] Li, D., and Dhir, V. K., 2007, “Numerical Study of Single Bubble Dynamics During Flow Boiling,” J. Heat Transfer, **129**(7), pp. 864–876.

[17] Wu, J., and Dhir, V. K., 2010, “Numerical Simulations of the Dynamics and Heat Transfer Associated With a Single Bubble in Subcooled Pool Boiling,” J. Heat Transfer, **132**(11), p. 111501.

[18] Wu, J., and Dhir, V. K., 2011, “Numerical Simulation of Dynamics and Heat

Transfer Associated With a Single Bubble in Subcooled Boiling and in the Presence of Noncondensables," J. Heat Transfer, **133**(4), p. 041502.

[19] Kern, J., and Stephan, P., 2003, "Theoretical Model for Nucleate Boiling Heat and Mass Transfer of Binary Mixtures," J. Heat Transfer, **125**(6), pp. 1106–1115.

[20] Fuchs, T., Kern, J., and Stephan, P., 2006, "A Transient Nucleate Boiling Model Including Microscale Effects and Wall Heat Transfer," J. Heat Transfer, **128**(12), pp. 1257–1265.

[21] Utaka, Y., Hu, K., Chen, Z., and Morokuma, T., 2018, "Measurement of Contribution of Microlayer Evaporation Applying the Microlayer Volume Change during Nucleate Pool Boiling for Water and Ethanol," Int. J. Heat Mass Transf., **125**, pp. 243–247.

[22] Rohsenow, W. M., 1952, "A Method of Correlating Heat Transer Data for Surface Boiling of Liquids," J. Heat Transfer, **74**, pp. 969–976.

[23] Pioro, I. l., 1999, "Experimental Evaluation of Constants for the Rohsenow Pool Boiling Correlation," Int. J. Heat Mass Transf., **42**(11), pp. 2003–2013.

[24] Levy, S., 1959, "Generalized Correlation of Boiling Heat Transfer," J. Heat Transfer, **81**(1), pp. 37–42.

[25] Kim, J., 2009, "Review of Nucleate Pool Boiling Bubble Heat Transfer Mechanisms," Int. J. Multiph. Flow, **35**(12), pp. 1067–1076.

[26] Gaertner, R. F., 1965, "Photographic Study of Nucleate Pool Boiling on a Horizontal Surface," J. Heat Transfer, **87**(1), pp. 17–27.

[27] Son, G., Ramanujapu, N., and Dhir, V. K., 2002, "Numerical Simulation of Bubble Merger Process on a Single Nucleation Site During Pool Nucleate Boiling," J. Heat Transfer, **124**(1), pp. 51–62.

[28] Mukherjee, A., and Dhir, V. K., 2004, "Study of Lateral Merger of Vapor Bubbles During Nucleate Pool Boiling," J. Heat Transfer, **126**(6), pp. 1023–1039.

[29] Banerjee, D., and Dhir, V. K., 2001, "Study of Subcooled Film Boiling on a Horizontal Disc:1 Part 2—Experiments," J. Heat Transfer, **123**(2), pp. 285–293.

[30] Hesse, G., Sparrow, E. M., and Goldstein, R. J., 1976, "Influence of Pressure on Film Boiling Heat Transfer," J. Heat Transfer, **98**(2), pp. 166–172.

[31] Lienhard, J. H., and Dhir, V. K., 1973, "Hydrodynamic Prediction of Peak Pool-Boiling Heat Fluxes from Finite Bodies," J. Heat Transfer, **95**(2), pp. 152–158.

[32] Kandlikar, S. G., 2001, "A Theoretical Model to Predict Pool Boiling CHF Incorporating Effects of Contact Angle and Orientation," J. Heat Transfer, **123**(6), pp. 1071–1079.

[33] Kandlikar, S. G., 2020, "Evaporation Momentum Force and Its Relevance to Boiling Heat Transfer," J. Heat Transfer, **142**(10), p. 100801.

[34] Warrier, G. R., and Dhir, V. K., 2006, "Heat Transfer and Wall Heat Flux Partitioning During Subcooled Flow Nucleate Boiling—A Review," J. Heat Transfer, **128**(12), pp. 1243–1256.

[35] Jones, B. J., McHale, J. P., and Garimella, S. V., 2009, "The Influence of Surface Roughness on Nucleate Pool Boiling Heat Transfer," J. Heat Transfer, **131**(12), p.

121009.

[36] Kim, J., Jun, S., Lee, J., Godinez, J., and You, S. M., 2017, “Effect of Surface Roughness on Pool Boiling Heat Transfer of Water on a Superhydrophilic Aluminum Surface,” J. Heat Transfer, **139**(10), p. 101501.

[37] Nakayama, W., Daikoku, T., Kuwahara, H., and Nakajima, T., 1980, “Dynamic Model of Enhanced Boiling Heat Transfer on Porous Surfaces—Part I: Experimental Investigation,” J. Heat Transfer, **102**(3), pp. 445–450.

[38] Li, C., and Peterson, G. P., 2007, “Parametric Study of Pool Boiling on Horizontal Highly Conductive Microporous Coated Surfaces,” J. Heat Transfer, **129**(11), pp. 1465–1475.

[39] Cooke, D., and Kandlikar, S. G., 2011, “Pool Boiling Heat Transfer and Bubble Dynamics Over Plain and Enhanced Microchannels,” J. Heat Transfer, **133**(5), p. 052902.

[40] Rahman, M. M., Pollack, J., and McCarthy, M., 2015, “Increasing Boiling Heat Transfer Using Low Conductivity Materials,” Sci. Rep., **5**(1), p. 13145.

[41] Jo, H., Ahn, H. S., Kang, S., and Kim, M. H., 2011, “A Study of Nucleate Boiling Heat Transfer on Hydrophilic, Hydrophobic and Heterogeneous Wetting Surfaces,” Int. J. Heat Mass Transf., **54**(25–26), pp. 5643–5652.

[42] Betz, A. R., Xu, J., Qiu, H., and Attinger, D., 2010, “Do Surfaces with Mixed Hydrophilic and Hydrophobic Areas Enhance Pool Boiling?,” Appl. Phys. Lett., **97**(14), p. 141909.

[43] Frankiewicz, C., and Attinger, D., 2017, "On Temporal Biphilicity: Definition, Relevance, and Technical Implementation in Boiling Heat Transfer," J. Heat Transfer, **139**(11), p. 111511.

[44] Shen, B., Yamada, M., Hidaka, S., Liu, J., Shiomi, J., Amberg, G., Do-Quang, M., Kohno, M., Takahashi, K., and Takata, Y., 2017, "Early Onset of Nucleate Boiling on Gas-Covered Biphilic Surfaces," Sci. Rep., **7**(1), p. 2036.

[45] Wang, C. H., and Dhir, V. K., 1993, "Effect of Surface Wettability on Active Nucleation Site Density During Pool Boiling of Water on a Vertical Surface," J. Heat Transfer, **115**(3), pp. 659–669.

[46] Yamada, M., Shen, B., Imamura, T., Hidaka, S., Kohno, M., Takahashi, K., and Takata, Y., 2017, "Enhancement of Boiling Heat Transfer under Sub-Atmospheric Pressures Using Biphilic Surfaces," Int. J. Heat Mass Transf., **115**, pp. 753–762.

[47] Shen, B., Yamada, M., Mine, T., Hidaka, S., Kohno, M., Takahashi, K., and Takata, Y., 2018, "Depinning of Bubble Contact Line on a Biphilic Surface in Subatmospheric Boiling: Revisiting the Theories of Bubble Departure," Int. J. Heat Mass Transf., **126**, pp. 715–720.

[48] Lemmon, E. W., and Ian H. Bell, Huber, M. L., and McLinden, M. O., 2018, "NIST Standard Reference Database 23: Reference Fluid Thermodynamic and Transport Properties-REFPROP, Version 10.0, National Institute of Standards and Technology."

[49] Takata, Y., Hidaka, S., and Uraguchi, T., 2006, "Boiling Feature on a Super

Water-Repellent Surface," Heat Transf. Eng., **27**(8), pp. 25–30.

[50] Shen, B., Liu, J., Amberg, G., Do-Quang, M., Shiomi, J., Takahashi, K., and Takata, Y., 2020, "Contact-Line Behavior in Boiling on a Heterogeneous Surface: Physical Insights from Diffuse-Interface Modeling," Phys. Rev. Fluids, **5**(3), p. 033603.

Table captions

Table 1 Thermophysical properties of water at different pressures [48]

Figure captions

Figure 1 Schematic illustration of the boiling test setup

Figure 2 Test surface used in the present study: (a) fabrication of the dimpled biphilic surface; (b) photograph of the surface showing an unstaggered array of uniform cavities (yellow bar: 10 mm); and (c) digital microscope images of the uncoated and coated cavity bottom walls (yellow bars: 200 μm)

Figure 3 Boiling curves for the plain copper surface at different pressures P=101.3 kPa and 9.1 kPa

Figure 4 Boiling curves for the biphilic surface without dimple cavities at different pressures P=14.3 kPa, 9.5 kPa, and 7.8 kPa

Figure 5 Heat transfer enhancement ratio h/h_R of the flat biphilic surface under low pressures of P=14.3 kPa, 9.5 kPa, and 7.8 kPa.

Figure 6 Boiling curves for the biphilic surface with dimple cavities at different pressures P=14.4 kPa, 9.5 kPa, and 7.8 kPa

Figure 7 Heat transfer enhancement ratio h/h_R of the dimpled biphilic surface under low pressures of P=14.4 kPa, 9.5 kPa, and 7.8 kPa

Figure 8 Test surface used for visualization of bubble dynamics. (a) The surface was comprised of two dimple cavities (yellow bar: 10 mm), and (b) the insides of the cavities of different depths were coated by hydrophobic PTFE coatings

Figure 9 High-speed images depicting bubble departure (ΔT_{sat}=7.9 K) from the flat surface coated with a single hydrophobic spot with diameter L=1.8 mm, at (a) P=100.8 kPa and (b) P=25.3 kPa

Figure 10 High-speed images depicting bubble departure (ΔT_{sat}=8.4 K) from the surface fabricated with two hydrophobic-coated ⌀1.8-mm cavities with various depths z_1=1.0 mm and z_2=0.5 mm, at (a) P=101.4 kPa and (b) P=25.4 kPa

Figure 11 Measurements of the bubble departure diameter D_b as a function of pressure from the hydrophobic spot (1.8 mm in diameter) on the flat surface of superheat ΔT_{sat}=7.9 K

Figure 12 Bubble departure from the flat biphilic surface with (a) pinned contact line and (b) depinned contact line

Figure 13 Measurements of the bubble departure diameter D_b as a function of pressure from the hydrophobic-coated ⌀1.8-mm cavities with various depths, (a) z_1=1.0 mm and (b) z_2=0.5 mm, under the superheat ΔT_{sat}=8.4 K

Figure 14 Bubble departure from the dimpled biphilic surface under (a) contact-line pinning and (b) secondary contact-line pinning

Figure 15 Effect of hydrophobic dimple structures to trap residual vapor after bubble departure. The horizontal axis represents the cavity depth, and the vertical axis the reduced pressure P/P^*

Figure S1 Measurement uncertainties (@68% confidence level) for the heat flux q, surface superheat ΔT_{sat}, and heat transfer coefficient h

Table 1 Thermophysical properties of water at different pressures [48]

P_{sat} (kPa)	T_{sat} (°C)	λ_l (W/m K)	ϱ_l (kg/m³)	ϱ_v (kg/m³)	h_{lv} (kJ/kg)	μ_l (μPa s)	σ (mN/m)	$c_{p,l}$ (kJ/kg K)	Pr_l (-)
101.3	100.0	0.679	958.37	0.5977	2256.44	281.8	58.917	4.2156	1.75
14.3	53.0	0.647	986.62	0.0954	2374.68	520.6	67.441	4.1825	3.37
9.5	44.8	0.637	990.25	0.0650	2394.47	598.1	68.809	4.1803	3.92
7.8	41.0	0.632	991.78	0.0540	2403.46	640.5	69.429	4.1798	4.24

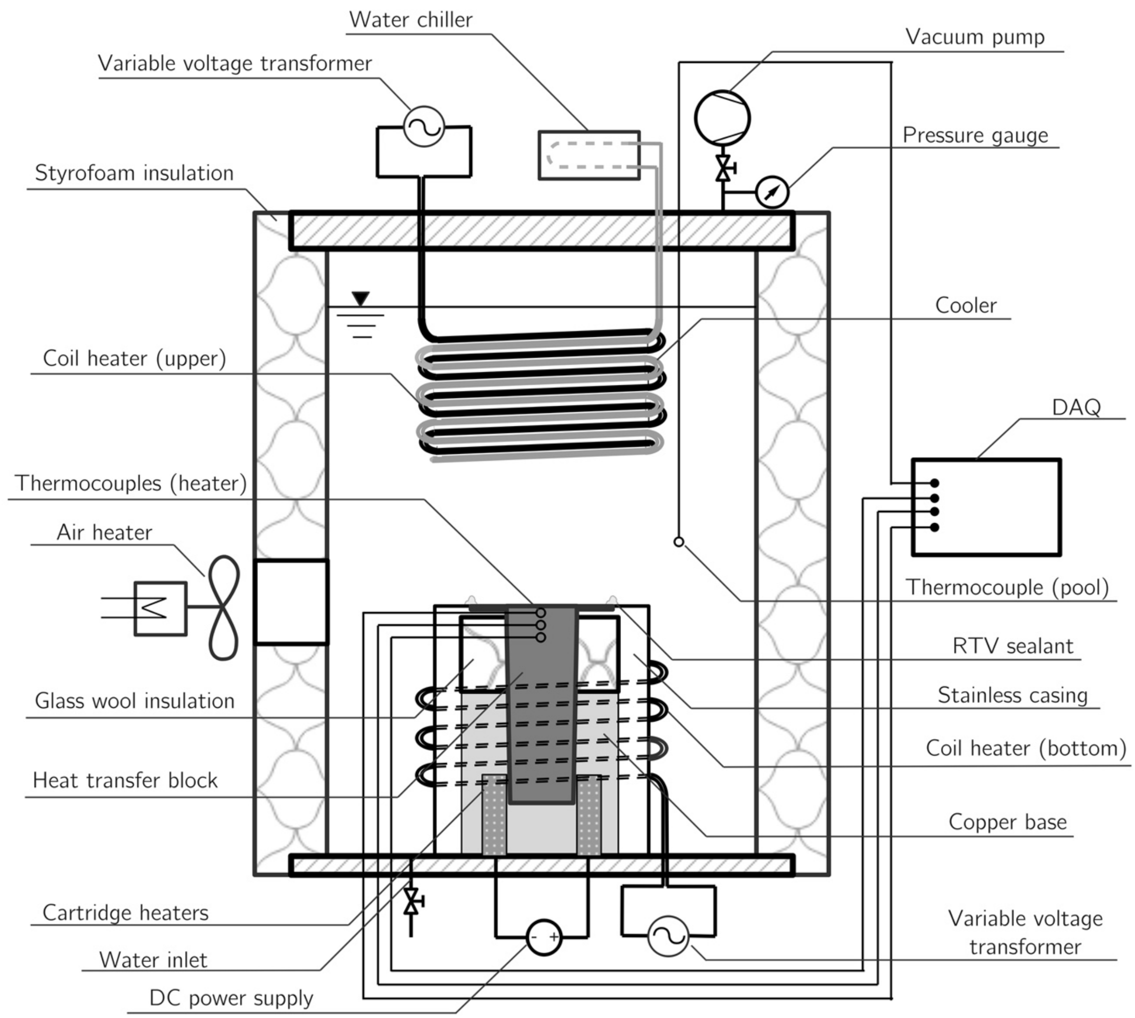
Water chiller
Vacuum pump
Variable voltage transformer
Pressure gauge
Styrofoam insulation
Cooler
Coil heater (upper)
DAQ
Thermocouples (heater)
Air heater
Thermocouple (pool)
RTV sealant
Stainless casing
Glass wool insulation
Coil heater (bottom)
Heat transfer block
Copper base
Cartridge heaters
Variable voltage transformer
Water inlet
DC power supply

Fig. 1

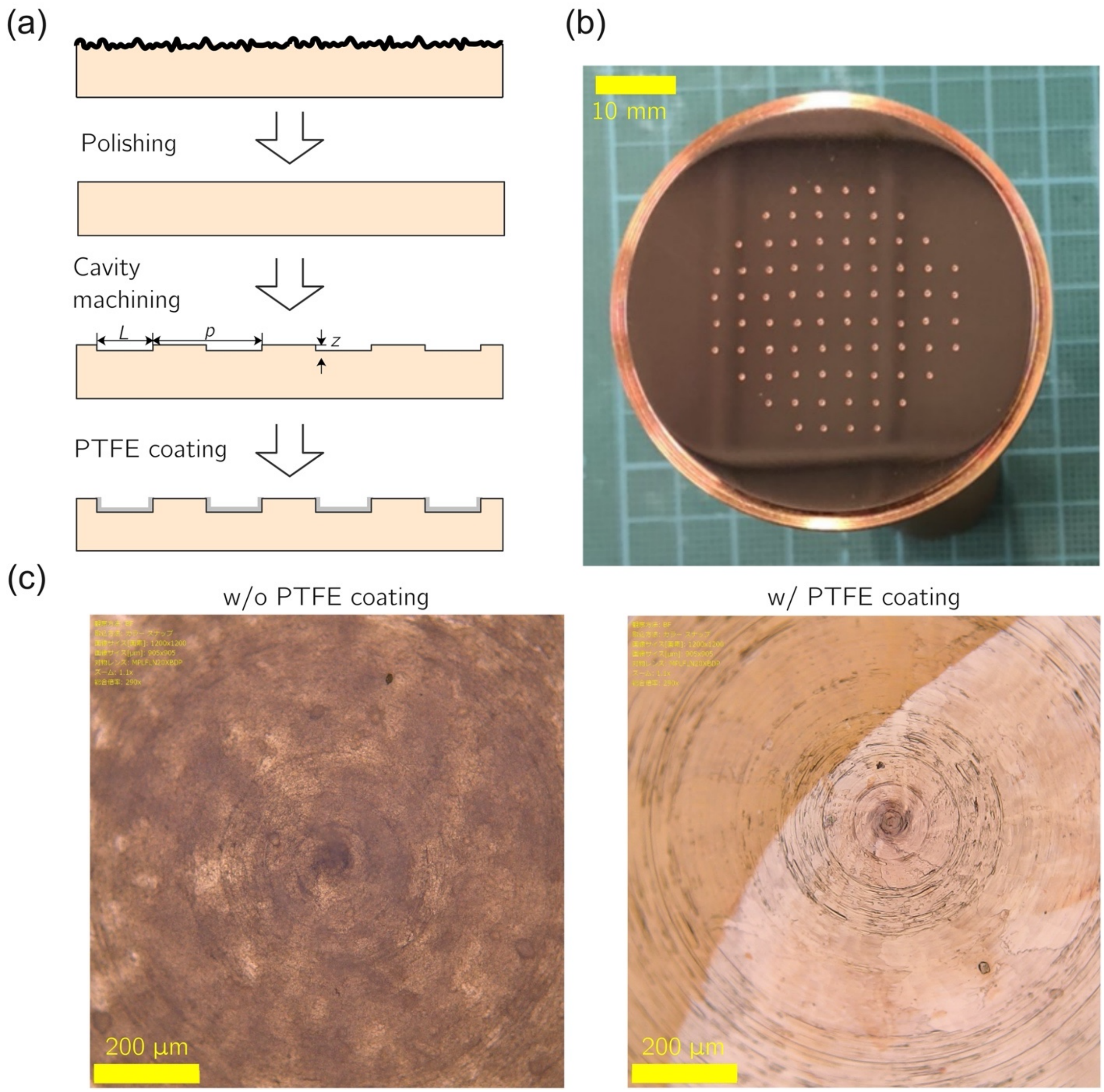
(a)
Polishing
Cavity machining
L
p
z
PTFE coating
(b)
10 mm
(c)
w/o PTFE coating
w/ PTFE coating
200 µm
200 µm

Fig. 2

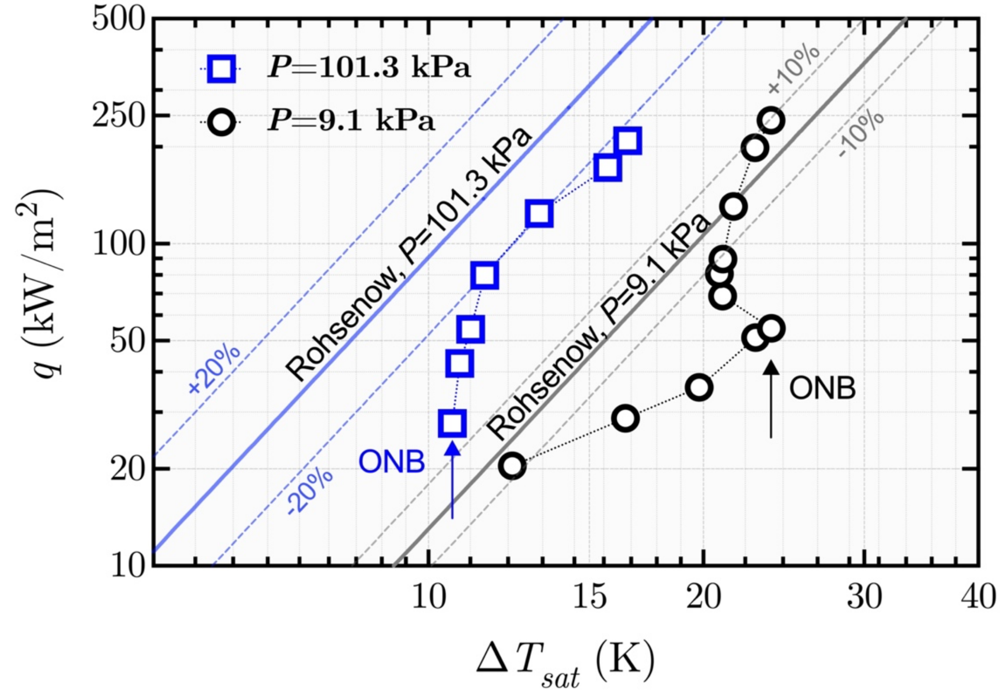

P=101.3 kPa
P=9.1 kPa
Rohsenow, P=101.3 kPa
Rohsenow, P=9.1 kPa
+20%
-20%
+10%
-10%
ONB
ONB
q (kW/m^2)
ΔT_{sat} (K)
500
250
100
50
20
10
10
15
20
30
40

822

823 Fig. 3

824

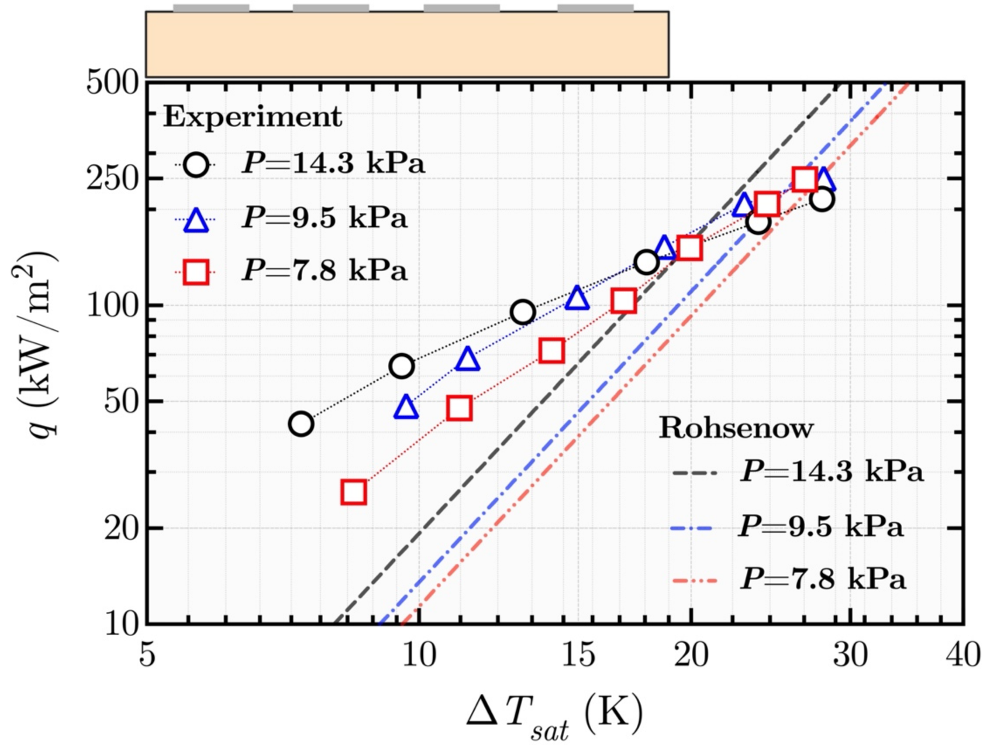

Experiment
P=14.3 kPa
P=9.5 kPa
P=7.8 kPa
Rohsenow
P=14.3 kPa
P=9.5 kPa
P=7.8 kPa
q (kW/m²)
ΔT_sat (K)
500
250
100
50
20
10
5
10
15
20
30
40

825 Fig. 4

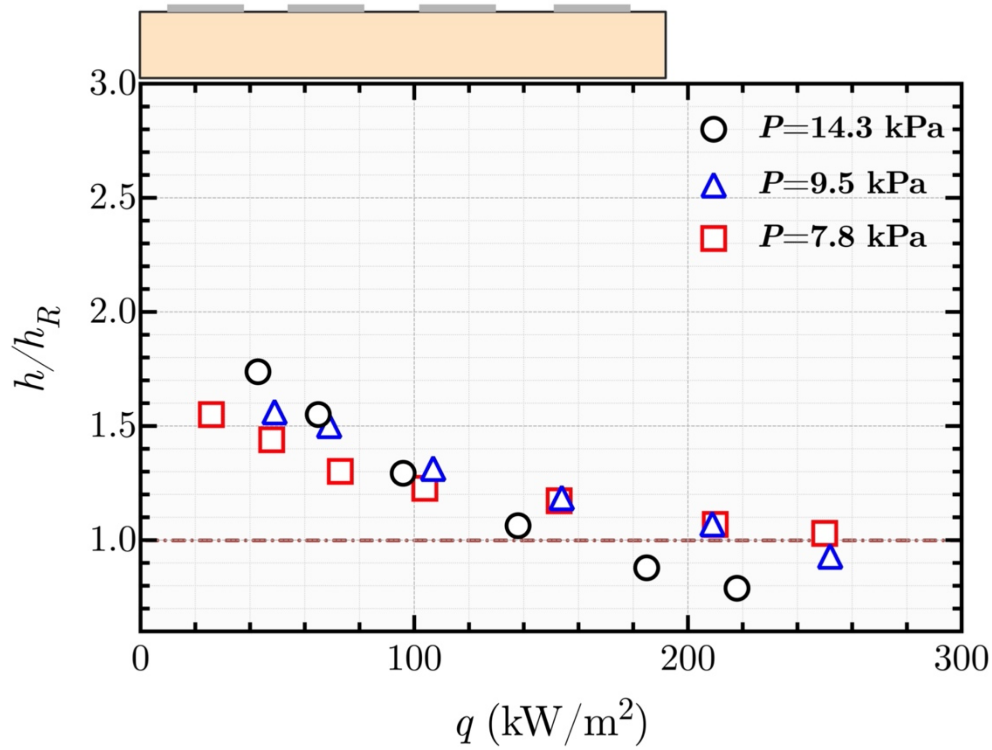

Fig. 5

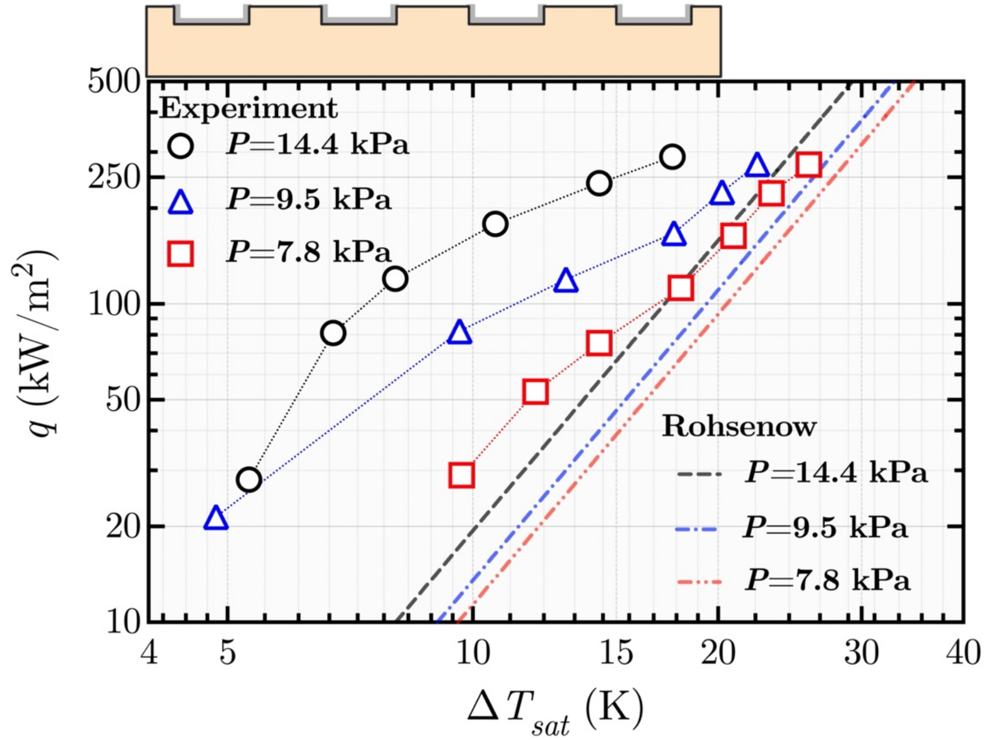
Experiment
P=14.4 kPa
P=9.5 kPa
P=7.8 kPa
Rohsenow
P=14.4 kPa
P=9.5 kPa
P=7.8 kPa
q (kW/m^2)
ΔT_{sat} (K)
500
250
100
50
20
10
4
5
10
15
20
30
40

Fig. 6

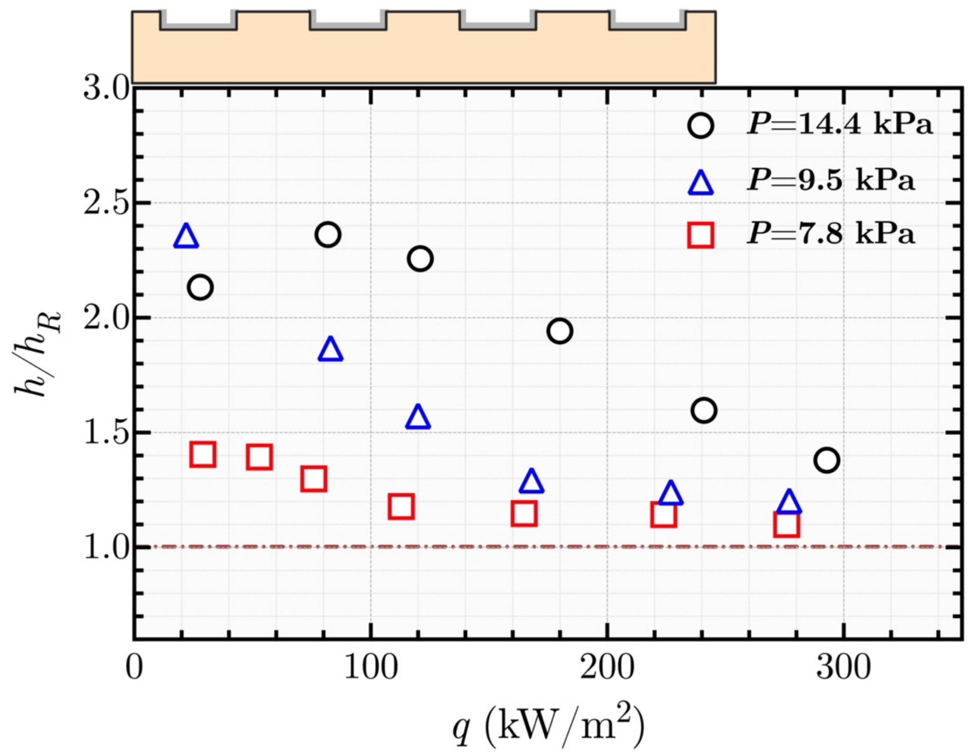

Fig. 7

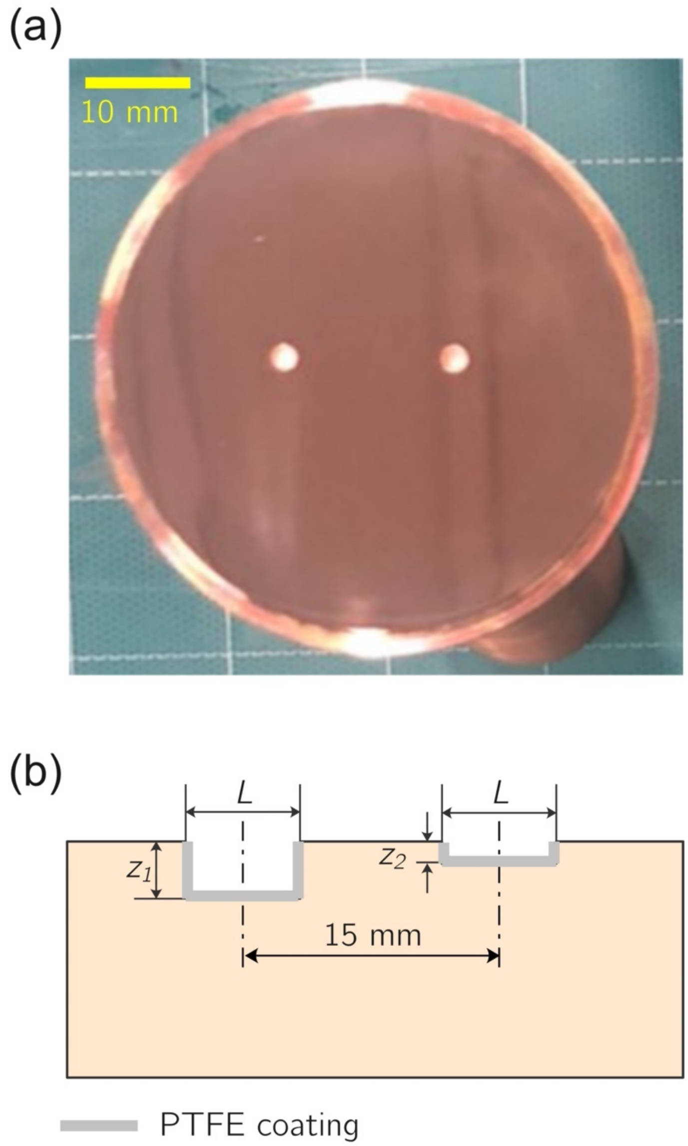

832

833 Fig. 8

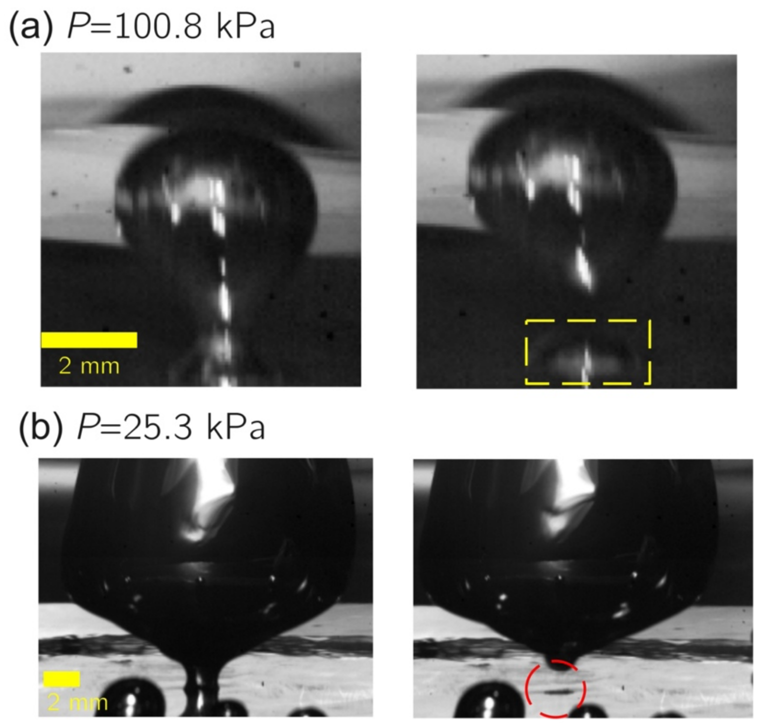

Fig. 9

836
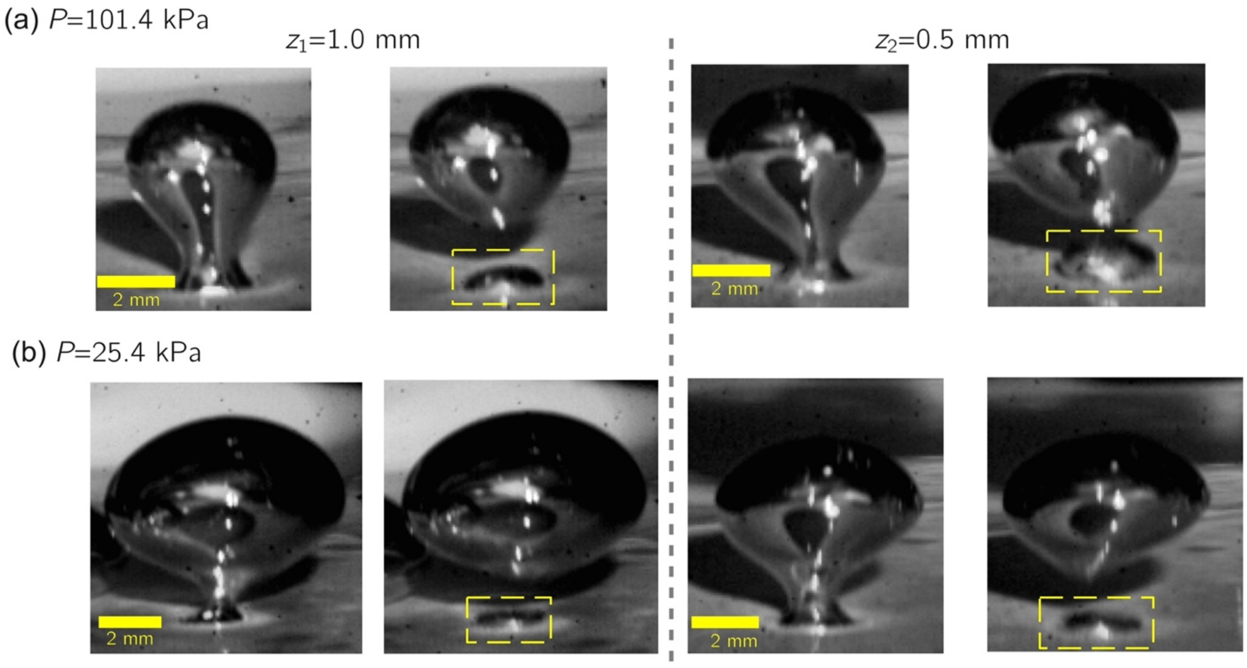

837 Fig. 10

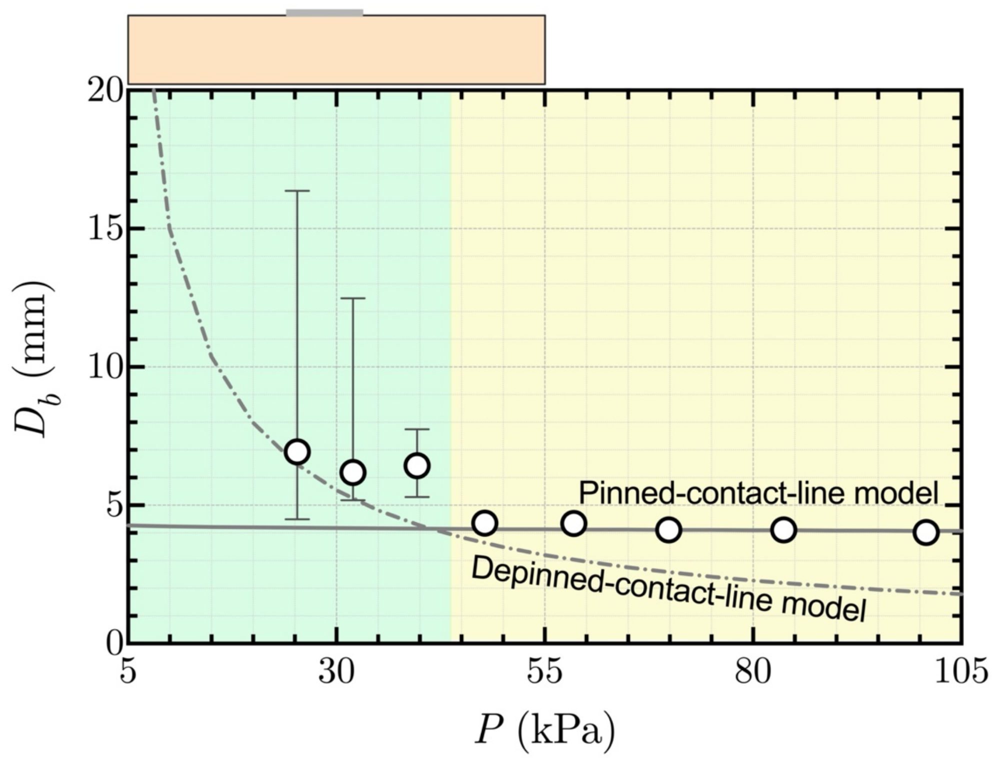

838

839 Fig. 11

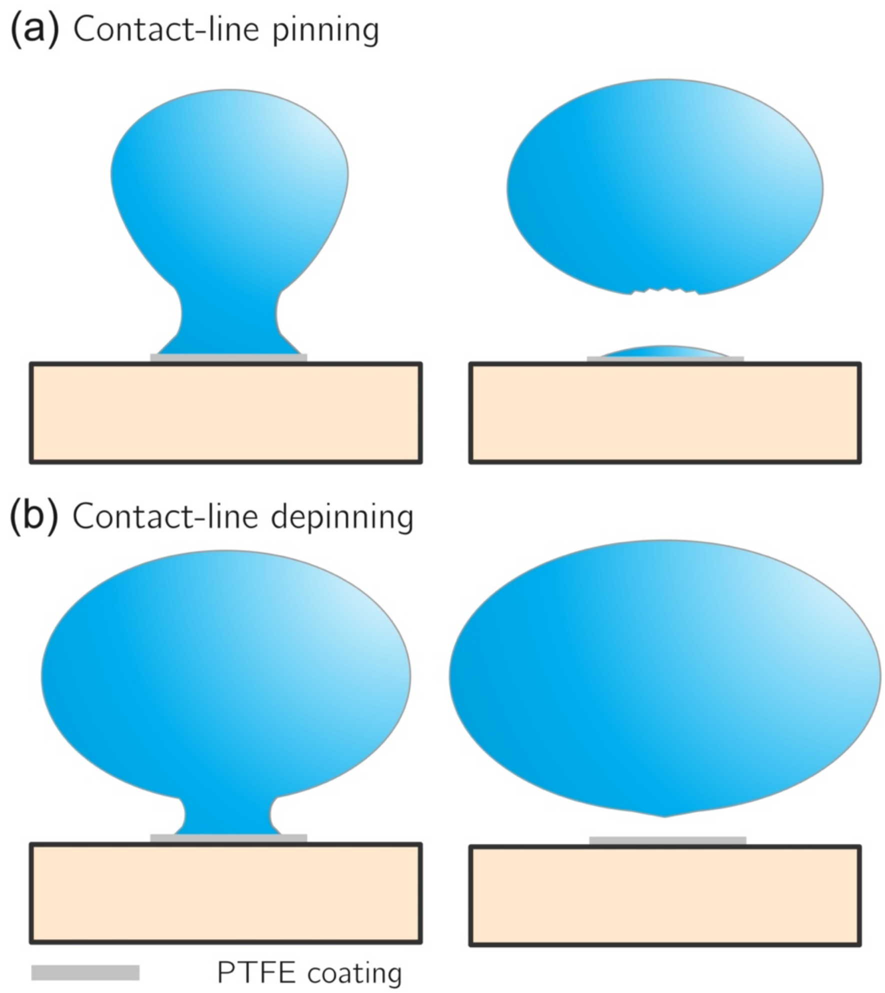

840

841 Fig. 12

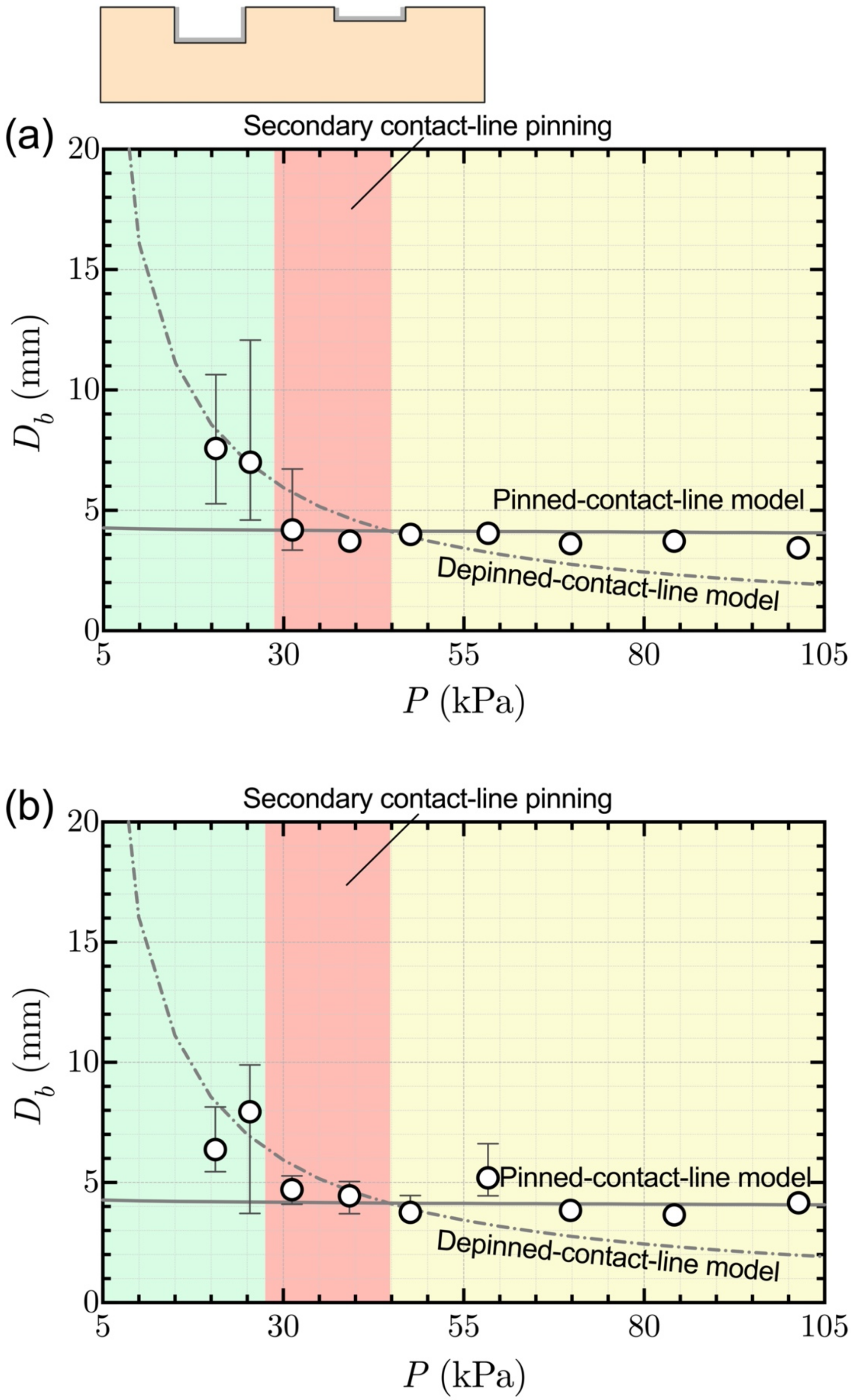
(a)
Secondary contact-line pinning
Pinned-contact-line model
Depinned-contact-line model
D_b (mm)
P (kPa)
(b)
Secondary contact-line pinning
Pinned-contact-line model
Depinned-contact-line model
D_b (mm)
P (kPa)

Fig. 13

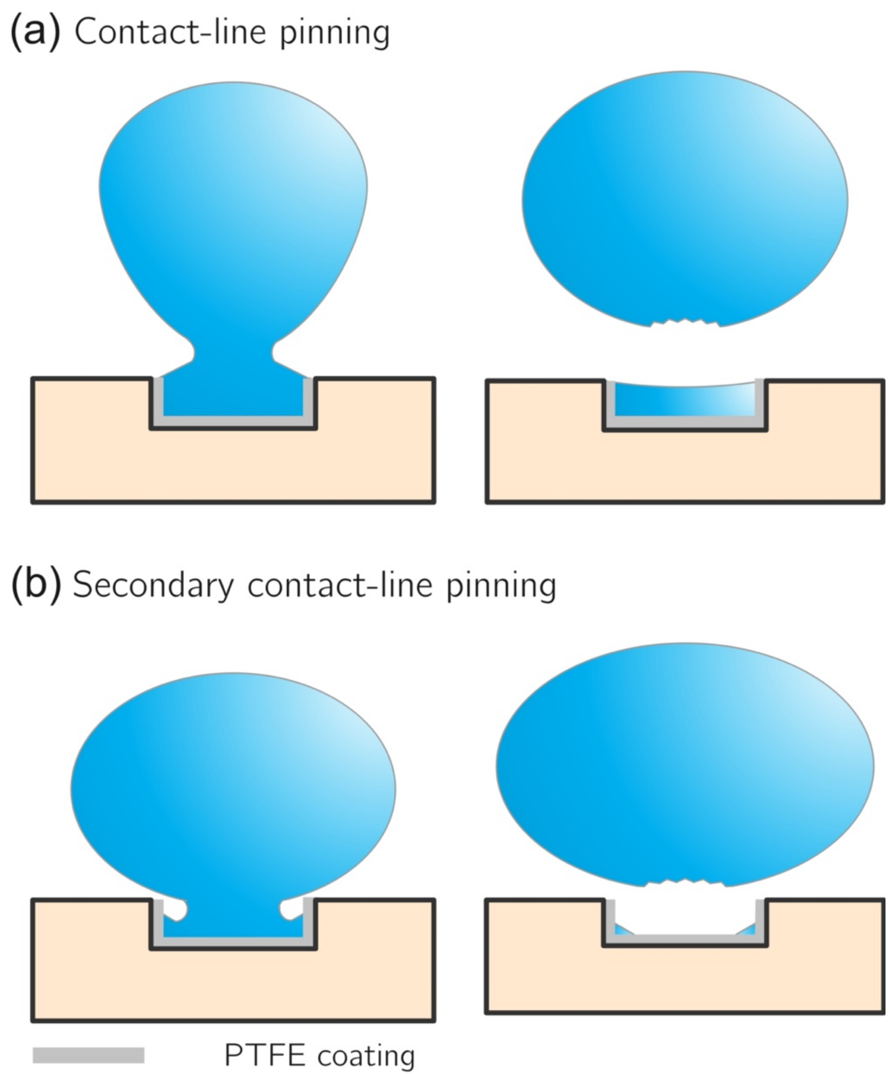
(a) Contact-line pinning
(b) Secondary contact-line pinning
PTFE coating

Fig. 14

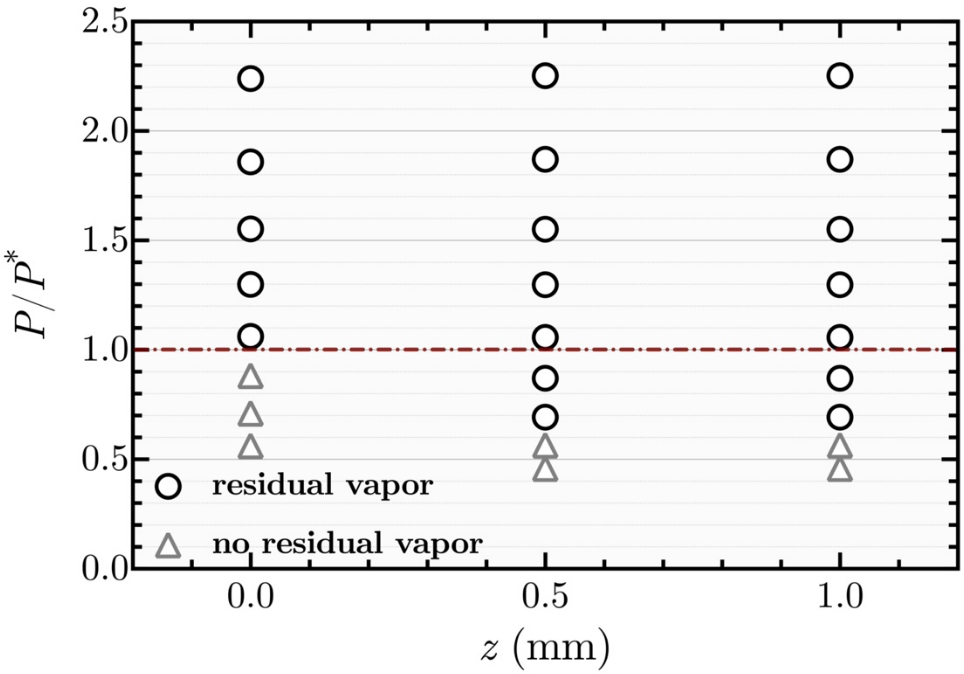

2.5
2.0
1.5
1.0
0.5
0.0
P/P^*
residual vapor
no residual vapor
0.0
0.5
1.0
z (mm)

Fig. 15

Supplemental Material

Limited Enhancement of Subatmospheric Boiling on Treated Structured Surfaces with Biphilic Pattern

Biao Shen[1]

Degree Programs in Systems and Information Engineering
The University of Tsukuba
Tennodai 1-1-1, Tsukuba 305-8573, Japan
b.shen@kz.tsukuba.ac.jp

Naoki Iwata

Department of Mechanical Engineering
Kyushu University
744 Motooka, Nishi-ku, Fukuoka 819-0395, Japan
n.iwata@heat.mech.kyushu-u.ac.jp

Sumitomo Hidaka

Department of Mechanical Engineering
Kyushu University
744 Motooka, Nishi-ku, Fukuoka 819-0395, Japan
hidaka@mech.kyushu-u.ac.jp

Koji Takahashi

Department of Aeronautics and Astronautics
Kyushu University
744 Motooka, Nishi-ku, Fukuoka 819-0395, Japan
takahashi@aero.kyushu-u.ac.jp

Yasuyuki Takata

Department of Mechanical Engineering
Kyushu University
744 Motooka, Nishi-ku, Fukuoka 819-0395, Japan
School of Engineering, The University of Edinburgh
The King's Buildings, Mayfield Road, Edinburgh EH9 3JL, United Kingdom
takata@mech.kyushu-u.ac.jp

[1] To whom correspondence should be addressed

881 The measurement uncertainties for surface superheat ΔT_{sat}, heat flux q, and heat

882 transfer coefficient h in the present study are shown in Fig. S1.

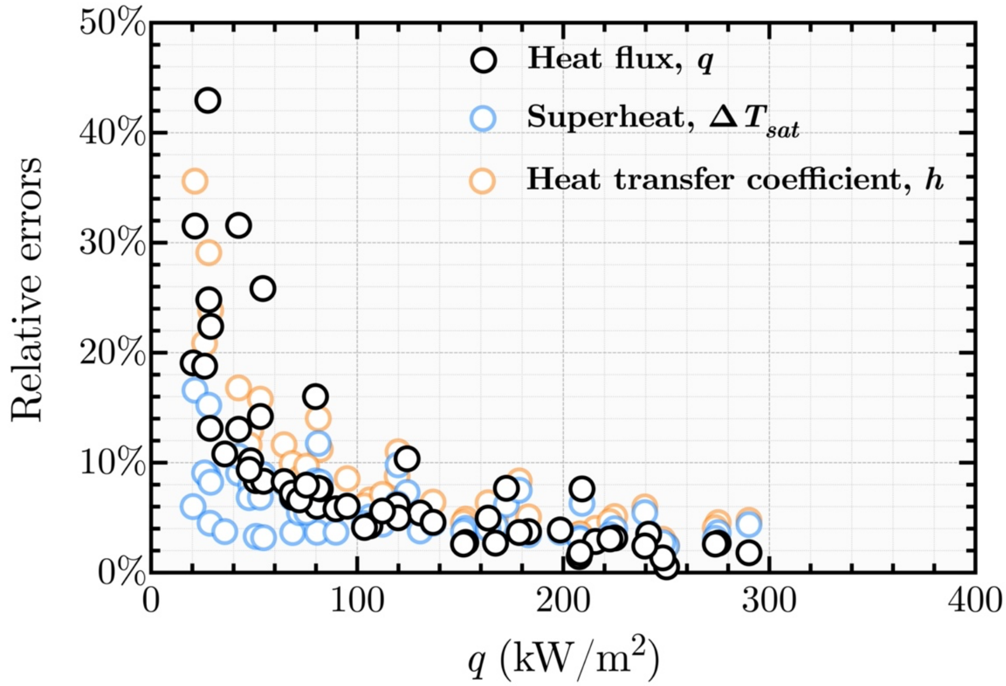

883

884 Figure S1 Measurement uncertainties (@68% confidence level) for the heat flux q, surface superheat ΔT_{sat},

885 and heat transfer coefficient h